Inverted catenoid as a fluid membrane with two points pulled together

Pavel Castro-Villarreal and Jemal Guven
Instituto de Ciencias Nucleares, Universidad Nacional Autónoma de México, Apdo. Postal 70-543, 04510 México, DF, Mexico
(Received 13 February 2007; published 27 July 2007)

Under inversion in any (interior) point, a catenoid transforms into a deflated compact geometry which touches at two points (its poles). The catenoid is a minimal surface and, as such, is an equilibrium shape of a symmetric fluid membrane. The conformal symmetry of the Hamiltonian implies that inverted minimal surfaces are also equilibrium shapes. However, they will exhibit curvature singularities at their poles. Such singularities are the geometrical signature of the external forces required to pull the poles together. These forces will set up stresses in the inverted shapes. Tuning the force corresponds geometrically to the translation of the point of inversion. For any fixed surface area, there will be a maximum force. The associated shape is a symmetric discocyte. Lowering the external force will induce a transition from the discocyte to a cup-shaped stomatocyte.

DOI: 10.1103/PhysRevE.76.011922 PACS number(s): 87.16.Dg, 46.70.Hg

I. INTRODUCTION

Biological membranes are fluid bilayers whose mechanical properties are described on mesoscopic scales by a bending energy quadratic in extrinsic curvature [1–4]. If bilayer asymmetry or constraints are ignored, this energy is invariant under the global conformal transformations of three-dimensional space [5–7]. Thus the bending energy is not only independent of the size of the membrane, it is unchanged under inversion in any point, $\mathbf{x}\rightarrow\mathbf{x}/|\mathbf{x}|^2$. As a consequence, every equilibrium configuration has a counterpart related to it by inversion which is also an equilibrium. Remarkably, this apparently unnatural symmetry does have physical consequences.

In practice, what one does is pair inversions in special conformal transformations which can be treated perturbatively. The study of inversion in its own right, however, lies beyond the reach of perturbation theory. Shapes do not simply get distorted, they may find themselves distorted beyond recognition; even their topology might change. If the point of inversion lies on the surface, this point gets consigned to infinity. Remote points on the surface, on the other hand, get mapped into a neighborhood of the origin; what is more, the geometry will generally exhibit curvature singularities there. The important point is that two shapes related by inversion will generally describe very different physical conditions. The singularities are a signal that localized external forces are operating.

In this paper, we will examine some of the physical implications of this, largely unexplored, nonperturbative aspect of conformal symmetry. We are interested, in particular, in the physical interpretation of the singularities that arise. We will look only at axially symmetric shapes. This would be very restrictive if we were to limit ourselves to looking at compact isolated geometries without internal or external constraints: the only equilibrium geometries of this kind are spheres and Clifford torii (ratio of the wheel to tube radius of $\sqrt{2}$).

Neither spheres nor torii offer surprises under inversion. The catenoid is also an isolated axially symmetric equilibrium geometry. Because it is infinite, however, the catenoid will map under inversion in any point which is not on the surface to a compact geometry. The two distal regions of the catenoid get mapped to the point of inversion. Thus the north and south poles of this geometry touch. However, they do so in such a way that the geometry possesses a tangent plane at these points so that it is appropriate to think of the topology as spherical. If, in particular, the catenoid is inverted in its center of symmetry, the transformed geometry is a symmetric biconcave discocyte.

Physically, it is clear that these deflated equilibria exist only if there are external forces counteracting the tendency to inflate. For, in the absence of constraints, one would expect the geometry to equilibrate by inflating into a sphere.

In general, external forces will act as sources of stress in the membrane [8]. The appropriate way to quantify the connection is to describe the geometry in terms of a conserved stress tensor [9,10]. In a fluid membrane this tensor depends only on the local geometry. In a catenoid formed by an ideal fluid membrane the stress vanishes [11]. However, there will be stress in its counterpart under inversion. Inversion will generally introduce stress, whether or not the geometry is singular.

The value of knowing the stress tensor in this context is that if we integrate an appropriate projection of it along a closed curve surrounding one of the poles we can identify the external force acting at that point. The integral will vanish unless the stress itself diverges there. But this can only happen if the geometry is singular there. We will show that, despite the apparent smoothness of an inverted catenoid at its poles, there is a curvature singularity lurking at these points: The two principal curvatures diverge logarithmically as they are approached [12]. These singularities are the geometrical manifestation of the localized external forces pulling the poles of the vesicle together. The existence of a connection between external forces and logarithmic singularities was originally pointed out by Podgornik, Svetina, and Žekš [13].

Shape changes are induced by tuning the external force. The easiest way to see this is to exploit once more the conformal symmetry of the problem: For tuning the force is related directly to the freedom to move the point of inversion. If this point is translated along the axis of symmetry, up-down symmetry is broken. The discocyte deforms con-

tinuously into a stomatocyte. One does need to recall that surface areas are not preserved under inversion. Thus, to follow the transition in a physically meaningful way, the geometries should be rescaled so that they possess the same area. The maximum external force consistent with this constraint produces the symmetric discocyte; a higher value presumably would rupture the membrane. For each value below this maximum, there is a unique axially symmetric geometry. As the force is reduced, the discocyte first inflates asymmetrically until a point is reached where it is identifiable as a stomatocyte; thereafter it deflates into an inverted sphere within a sphere. We have not performed a complete stability analysis; however, there are reasons to expect this description to be stable with respect to small perturbations breaking the axial symmetry.

The paper is organized as follows. In Sec. II we describe inverted minimal surfaces focusing on the stresses within them; in Sec. III we provide a detailed physical interpretation of the inverted catenoid. Some of these results were announced in [12]. We finish with a discussion and an outline of our plans for future work.

II. WILLMORE ENERGY AND INVERTED MINIMAL SURFACES

A parametric description of an embedded two-dimensional surface in three-dimensional space is provided by the mapping $(u^1,u^2)\rightarrow\mathbf{X}(u^1,u^2)$. The Willmore energy associated with this surface is given by

$$H[\mathbf{X}]=\int dA\left(K^{ab}-\frac{1}{2}g^{ab}K\right)\left(K_{ab}-\frac{1}{2}g_{ab}K\right), \tag{1}$$

where g_{ab} is the metric, K_{ab} is the extrinsic curvature tensor, and $K=g^{ab}K_{ab}$ is its trace (twice the mean curvature). dA is the induced element of area. This notation is summarized in Appendix A. $H[\mathbf{X}]$ is a measure of the energy associated with bending. This energy possesses one remarkable property: It is invariant with respect to the conformal transformations of the ambient space [5,14]. Thus $H[\mathbf{X}]$ is invariant not only under the transformations of the surface induced by the Euclidean motions, translations and rotations, it is also invariant under transformations preserving angles: Dilations $\mathbf{X}\rightarrow\lambda\mathbf{X}$ and inversion,

$$\mathbf{X}\rightarrow\frac{\mathbf{X}}{|\mathbf{X}|^2}. \tag{2}$$

Modulo, a topological contribution proportional to the Gauss-Bonnet invariant H, coincides with the Helfrich energy

$$H[\mathbf{X}]=\frac{1}{2}\int dA\ K^2. \tag{3}$$

There is only one local two-dimensional bending energy.

The surfaces which provide the equilibria of the energy (1) satisfy the Euler-Lagrange equation

$$-\nabla^2K+\frac{1}{2}(Kg_{ab}-2K_{ab})K^{ab}K=0, \tag{4}$$

where ∇^2 is the surface Laplacian compatible with the metric g_{ab}. It is clear that minimal surfaces, satisfying $K=0$, are solutions of Eq. (4). However, because of the conformal symmetry of the shape equation, these surfaces map under inversion to new solutions of Eq. (4). This is true not just infinitesimally but also for finite conformal transformations. In particular, it is true for inversion.

Let us first examine the behavior of minimal surfaces under inversion. In particular, let us first identify the equation satisfied by the transformed surface. It is well known that the principal curvatures transform under inversion by $C_I\rightarrow\bar{C}_I$, where (see, for example, [15])

$$\bar{C}_I=-|\mathbf{X}|^2\left(C_I-2\frac{(\mathbf{X}\cdot\mathbf{n})}{|\mathbf{X}|^2}\right). \tag{5}$$

Thus the transformed mean curvature $K=C_1+C_2$ is given by

$$\bar{K}=-|\mathbf{X}|^2\left(K-4\frac{(\mathbf{X}\cdot\mathbf{n})}{|\mathbf{X}|^2}\right). \tag{6}$$

We conclude from Eq. (6) that a surface satisfying

$$K=4\frac{\mathbf{X}\cdot\mathbf{n}}{|\mathbf{X}|^2} \tag{7}$$

is mapped under inversion to a minimal surface, and conversely. It is clear that the only minimal surfaces mapping to minimal surfaces are the planes through the origin.[1] If the origin itself lies on the surface, K will diverge there unless the surface aligns along $\mathbf{X}$ sufficiently fast as $|\mathbf{X}|\rightarrow 0$. While this is true if the original minimal surface has planar ends it is not true if the ends behave like a catenoid. Inverted minimal surfaces typically possess curvature singularities.

Inverted minimal surfaces also satisfy Eq. (4). Thus any solution to Eq. (7) is also a solution to Eq. (4). It is straightforward, but instructive, to confirm this fact with an explicit calculation: we note that, in modulo Eq. (7), we have

$$\partial_aK=\frac{4}{|\mathbf{X}|^2}\left(K_{ab}-\frac{1}{2}g_{ab}K\right)(\mathbf{X}\cdot\mathbf{e}^b). \tag{8}$$

This makes use of the Weingarten equations, $\partial_a\mathbf{n}=K_{ab}\mathbf{e}^b$. Equation (4) follows (except possibly at the origin) on using the Gauss equations, $\nabla_a\mathbf{e}_b=-K_{ab}\mathbf{n}$ as well as the contracted Codazzi-Mainardi equations,

$$\nabla_aK^{ab}-\nabla^bK=0. \tag{9}$$

Here ∇_a is the surface covariant derivative compatible with g_{ab}. Unlike minimal surfaces, the equilibrium of the inverted counterpart involves a nontrivial cancellation between the Laplacian of K and the terms cubic in K_{ab}. If the origin lies on the surface, however, Eq. (7) will not generally hold at

[1]Equation (7) can also be written as $\mathbf{n}\cdot[\nabla^2\mathbf{X}+4\mathbf{X}/|\mathbf{X}|^2]=0$. Note, however, that there are no solutions consistent with peeling off $\mathbf{n}$. Surfaces satisfying this equation can also be interpreted as the stationary configurations of the functional $H_1[\mathbf{X}]=\int dA/|\mathbf{X}|^4$.

this point and there will be a geometrical singularity there. In the following section we will show how to interpret this apparent pathology physically in terms of a localized external force acting on the membrane at this point.

Conserved stress tensor and Noether charges for the inverted minimal surfaces

The physical interpretation of geometrical singularities in the transformed geometry at the origin of inversion is facilitated by identifying a stress tensor with the geometry. This tensor is given in terms of the extrinsic curvature tensor by [9,10]

$$\mathbf{f}^a = K\left(K^{ab} - \frac{1}{2}g^{ab}K\right)\mathbf{e}_b - \partial^a K\mathbf{n}. \tag{10}$$

In equilibrium, $\mathbf{f}^a$ is conserved so that $\nabla_a \mathbf{f}^a = 0$. It is simple to check that the local conservation law does, in fact, reproduce the shape equation (4).

The transformed stress tensor under inversion is given by

$$\bar{\mathbf{f}}^a = |\mathbf{X}|^4\left[|\mathbf{X}|^2 \mathsf{R}\mathbf{f}^a + 4\left(K^{ab} - \frac{1}{2}g^{ab}K\right)\mathbf{f}_{b0}\right], \tag{11}$$

where

$$\mathsf{R}^{ij} = \delta^{ij} - 2\hat{X}^i\hat{X}^j$$

is a reflection in the plane orthogonal to $\mathbf{X}$, and

$$\mathbf{f}_0^a = (\mathbf{e}^a \cdot \mathbf{X})\mathbf{n} - (\mathbf{n} \cdot \mathbf{X})\mathbf{e}^a. \tag{12}$$

The role of $\mathbf{f}_0^a$ in the context of conformal symmetry has been noted elsewhere [16]. Curiously, it also has a role as an effective surface stress tensor for an external Laplace force [17].

In a minimal surface with $K=0$ the stress vanishes. However, it does not vanish in its inverted counterpart satisfying Eq. (7). The corresponding stress tensor is given by

$$\mathbf{f}^a = -\frac{4}{|\mathbf{X}|^2}\left(K^{ab} - \frac{1}{2}g^{ab}K\right)\mathbf{f}_{b0}. \tag{13}$$

It is also straightforward to demonstrate that $\mathbf{f}^a$ given by Eq. (13) is conserved if $\mathbf{X} \neq 0$: One uses Eq. (8) as well as the identity

$$\nabla_b \mathbf{f}_{0a} = g_{ab}\mathbf{n} + K_b{}^c[(\mathbf{X} \cdot \mathbf{e}_a)\mathbf{e}_c - (a \leftrightarrow c)], \tag{14}$$

satisfied by $\mathbf{f}_0^a$.

As noted in [12], a curvature singularity at a point will be associated with a source of stress at that point. Let Γ be any closed contour on the surface of the membrane encircling the point. Stoke's theorem applied to the conservation law implies that the closed line integral

$$\oint ds\, l^a \mathbf{f}_a \tag{15}$$

is a constant vector $\mathbf{F}$ along contours that are homotopically equivalent to Γ on this surface [8]. Here $\mathbf{l} = l^a\mathbf{e}_a$ is the normal to Γ tangent to the surface, and ds is the element of arc length along Γ. The set of values of $\mathbf{F}$ are the Noether charges associated with the translation invariance of the energy.

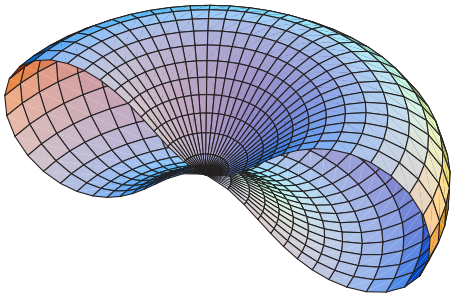

FIG. 1. (Color online) Section through symmetric biconcave discocyte.

If the conservation law is valid everywhere, $\mathbf{F}$ must vanish on any topologically trivial loop. This is the case for a membrane with spherical topology. Thus, if $\mathbf{F} \neq 0$ on such a loop, there must be a source of stress within it [8]. In particular, a distributional source of stress manifests itself in a curvature singularity which is picked up by the line integral. $\mathbf{F}$ is a reparametrization invariant measure of the strength of singularity.

Note also that the total external force acting on the membrane must vanish in equilibrium. Thus, in an axially symmetric membrane, the forces operating at the poles must be equal and opposite.

A concrete implementation of these ideas will be developed in the following section.

III. INVERSION OF CATENOIDS

Conformal invariance permits a remarkably simple construction of a two-parameter family of axially symmetric solutions of Eq. (4). Begin with a catenoid which solves the shape equation trivially as a minimal surface with $K=0$.

For a fixed axis of rotation, a catenoid $\Sigma_{(R_0,\xi_0)}$, is given as the level set $\Phi(R,Z)=0$ of the function[2]

$$\Phi(R,Z) = R - \frac{1}{R_0}\cosh(R_0 Z + \xi_0). \tag{16}$$

It is characterized by a scale $1/R_0$ and an offset ξ_0/R_0 along the axis. Thus any two catenoids are related by scaling and translation. They are the only nontrivial rotational minimal surfaces.

The image of the catenoid $\Sigma_{(R_0,\xi_0)}$ under inversion in the origin is the surface $\bar{\Sigma}_{(R_0,\xi_0)}$ described as the level set

$$\frac{R}{R^2+Z^2} - \frac{1}{R_0}\cosh\left(\frac{R_0 Z}{(R^2+Z^2)} + \xi_0\right) = 0. \tag{17}$$

This is a simple transcendental equation in the variables R and Z.

[2]Scaling the catenoid with an inverse length will give an inverted geometry with the "correct" dimensions.

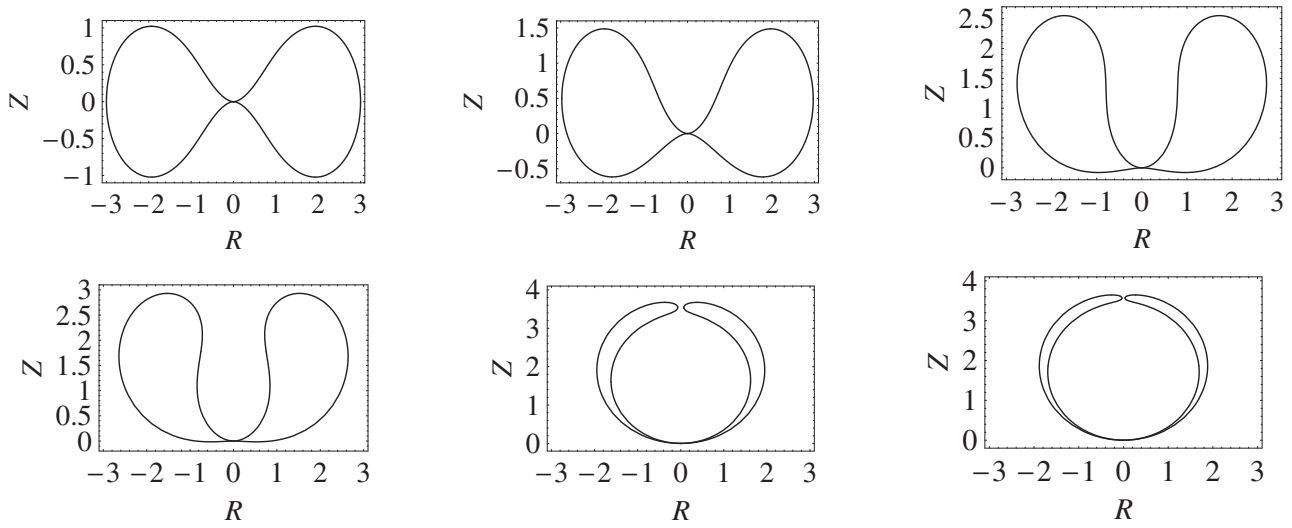

FIG. 2. Geometric profiles for $\xi_0=0$, 1, 2, 3, 50, and 100. The surface is generated by rotating the profile about the vertical axis. The area is normalized.

One particular solution, the symmetric biconcave discocyte with $\xi_0=0$, is illustrated in Fig. 1. The geometric profiles for several different values of ξ_0 are displayed in Fig. 2. Surface area is not preserved under inversion; thus, as we discuss below, these profiles have been rescaled so that they all possess the same surface area.

We note the following properties of these new surfaces.

(1) The geometry is bounded for all values of ξ_0. The circle $R=1/R_0 \cosh \xi_0$ on the plane $Z=0$ is mapped to the circle $R=R_0/\cosh \xi_0$ on the same plane. The remote regions of the catenoid map to the point of inversion. Thus the north and south poles of this geometry touch. As we will see, they do so with a common tangent plane $Z=0$. In this sense, the inverted surface does not self-intersect. The topology is spherical. However, there will be a singularity at the origin.

Generically, the behavior at the origin will not be so simple. Consider, for example, the fate of another simple geometry, the hyperboloid of revolution, under inversion in the origin. Asymptotically, the hyperboloid is conical. Because cones map to cones under inversion in the apex, the inverted geometry will be conical at the origin; it is not spherical. The existence of a tangent plane in the inverted catenoids is a consequence of the faster asymptotic growth rate (exponential) of the catenoid.

(2) When $\xi_0=0$, the surface is a biconcave discocyte possessing up-down symmetry. This symmetry is a consequence of the symmetry of the original catenoid with respect to the point of inversion.

(3) The symmetry is broken by translating the point of inversion along the axis. Beyond some critical value, $\xi_0^*=1.868$ discussed below, the lower concave region becomes vanishingly small: There is a transition from the symmetric biconcave discocyte to an asymmetrical stomatocyte.

(4) In the limit $\xi_0 \to \infty$, the stomatocyte degenerates into a completely deflated geometry consisting of a sphere within a sphere connected by an infinitesimal neck, a catenoid. It is possible to describe the complete sequence from discocyte to limiting deflated stomatocyte analytically.

It should be remarked that, technically, the lower concave region persists for all values of ξ_0; the ratio ξ_0/R_0 determines the position of the center along the axis; thus no matter how large a value we take for ξ_0, there always will be a region of the catenoid where Z is negative; this region will map to negative Z in the inverted geometry and will contain a concave component. Of course, as the profiles above clearly illustrate, while this concave region is always present, it becomes small in comparison with the overall size of the geometry. How small will be described quantitatively in our discussion of the isoperimetric ratio.

A. Isoperimetric ratio of the inverted shapes

To examine the geometry quantitatively, it is useful to introduce a parametric representation of the catenoid in terms of the angle that the tangent to the meridian makes with a plane of constant Z:

$$R(\Theta)=\frac{1}{R_0}\csc\Theta, \quad Z(\Theta)=\frac{1}{R_0}\ln\tan\Theta/2+\frac{\xi_0}{R_0}. \tag{18}$$

where Θ lies in the interval $[0,\pi]$. This angle also provides a parametrization of the inverted catenoid $\bar{\Sigma}$:

$$\bar{R}(\Theta)=\frac{R_0\sin\Theta}{1+\sin^2\Theta[\ln\tan(\Theta/2)+\xi_0]^2},$$

$$\bar{Z}(\Theta)=\frac{R_0\sin^2\Theta[\ln\tan(\Theta/2)+\xi_0]}{1+\sin^2\Theta[\ln\tan(\Theta/2)+\xi_0]^2}. \tag{19}$$

The interval of Θ does not change under inversion. A word of caution: Θ and its inverted counterpart $\bar{\Theta}$ are not the same angle, i.e., Θ has nothing to do with the angles which are preserved under conformal transformation.[3] While it might be more natural to parametrize the inverted surface by $\bar{\Theta}$, the

[3]More generally, $\bar{\mathbf{e}}_a\cdot\mathbf{k}\neq\mathbf{e}_a\cdot\mathbf{k}$, where $\mathbf{k}$ is a fixed unit vector.

advantage has to be weighed against the complicated form of the corresponding functional forms of $\bar{R}$ and $\bar{Z}$.

A straightforward calculation shows that the parametrization by Θ is isothermal. The metric on the inverted catenoid is described by the line element

$$ds^2 = R_0^2 \Omega^2(\Theta)[d\Theta^2 + \sin^2\Theta d\varphi^2], \tag{20}$$

where φ is the polar azimuthal angle, and the conformal factor Ω is given by

$$\Omega(\Theta)^{-1} = 1 + \sin^2\Theta\left(\log\tan\frac{\Theta}{2} + \xi_0\right)^2. \tag{21}$$

The area of the surface is given with respect to this parametrization by $A=4\pi R_0^2 \mathcal{A}(\xi_0)$, where

$$\mathcal{A}(\xi_0) = \frac{1}{2}\int_0^\pi d\Theta \sin\Theta\Omega(\Theta)^2, \tag{22}$$

with range $(0,\infty)$. The area of the surface is used to express R_0 as a function of ξ_0 for a fixed area A as $R_0(\xi_0) = \sqrt{A/4\pi\mathcal{A}(\xi_0)}$. The volume enclosed by the surface is given by $V=(4\pi R_0^3/3)\mathcal{V}(\xi_0)$, where

$$\mathcal{V}(\xi_0) = \frac{1}{2}\int_0^\pi d\Theta \sin^3\Theta\left[1 + \cos\Theta\left(\log\tan\frac{\Theta}{2} + \xi_0\right)\right]\Omega^3(\Theta), \tag{23}$$

and thus the isoperimetric ratio ν, defined by $\nu = V/V_A = 3\sqrt{4\pi}V/A^{3/2}$ where V_A is the volume of a sphere of surface area A, is given by

$$\nu(\xi_0) = \mathcal{V}(\xi_0)/\mathcal{A}(\xi_0)^{3/2}. \tag{24}$$

The maximum value $v=1$ is attained by a sphere. Clearly the constraint that the poles touch introduces bending energy. As a consequence the value $v=1$ is not attained in any equilibrium geometry with touching poles.

The isoperimetric ratio is plotted as a function of ξ_0 in Fig. 3(a). $v(\xi_0)$ possesses three extrema: Two maxima and one minimum. The maxima $v_{\max}=0.666$ occur when $\xi_0^* = \pm 1.868$. The corresponding geometry marks the transition from discocyte to stomatocyte (depicted in Fig. 2). The shallow local minimum $v_{\min}=0.648$ occurs when $\xi_0=0$, the symmetric biconcave geometry. We observe, in particular, the interesting fact that the maximally inflated geometry is not the symmetric discocyte. ν vanishes asymptotically in the limits $\xi_0 \to \pm\infty$. This property is evident in the corresponding profile (see Fig. 2).

We observe, in particular, that $v(\xi_0)$ may not be inverted for ξ_0 on the interval $\xi_0 \in [0,\infty)$. This indicates that it cannot be used in place of ξ_0 as the "order parameter" to describe the discocyte-stomatocyte transition. As we will see, the appropriate physical parameter is the Noether charge or external force $\mathbf{F}$. This physical interpretation will be developed in the following sections.

It was pointed out in the preceding section that, from a technical point of view, the geometry remains biconcave for all values of ξ_0. We will now demonstrate that one of the concave regions becomes vanishingly small when ξ_0 is larger

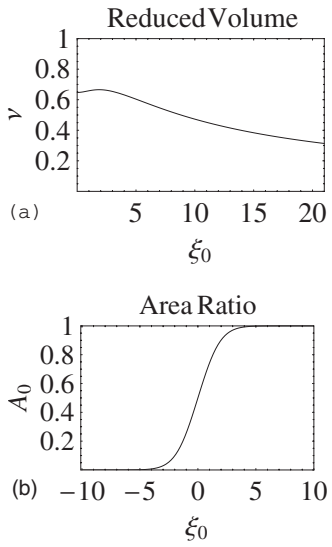

FIG. 3. (a) Isoperimetric ratio vs ξ_0; (b) area ratio vs ξ_0.

than the critical value $\xi_0^*=1.868$. To do this, we determine the fraction of surface area lying above $Z=0$. We thus define the ratio

$$\frac{A_0}{A} = \frac{1}{\mathcal{A}(\xi_0)}\int_{\Theta_0(\xi_0)}^\pi d\Theta \sin\Theta\Omega(\Theta), \tag{25}$$

where $\Theta_0(\xi_0)=2\arctan[\exp(-\xi_0)]$ is the tangent angle along the meridian where the surface intersects $Z=0$. For example, when $\xi_0=0$, $\theta_0(0)=\pi/2$ and the area ratio is one-half. Figure 3(b) illustrates clearly the rapid approach of the ratio to 1 above the critical value, ξ_0^*.

B. Curvature singularities

We expect a curvature singularity at the poles. This is because the only regular equilibrium geometries with spherical topology are the round spheres. We will now confirm that the geometries described by Eq. (17) are regular everywhere except at the poles where they display a (logarithmic) curvature singularity. The strength of this singularity will be related to the external force tethering the poles together.

In the case of the symmetric discocyte it is very simple to study this singular behavior analytically. To do this, note that, in the neighborhood of the origin, Eq. (17) is approximated by

$$\frac{1}{R} \approx \frac{1}{2R_0}\exp\left(\frac{R_0 Z}{R^2}\right) \tag{26}$$

which can be inverted for Z as a function of R,

$$\frac{Z}{R_0} \approx -\left(\frac{R}{R_0}\right)^2 \log\left(\frac{R}{2R_0}\right) \tag{27}$$

when $R \approx 0$. Whereas $Z_{,R}$ vanishes at $R=0$, it is clear that both the curvature along the meridian $C_\perp \approx Z_{,RR}$, as well as that along the parallel, $C_\parallel \approx Z_{,R}/R$, diverge logarithmically (see Appendix B). Indeed, $C_\parallel$ and $C_\perp$ exhibit identical logarithmic divergences:

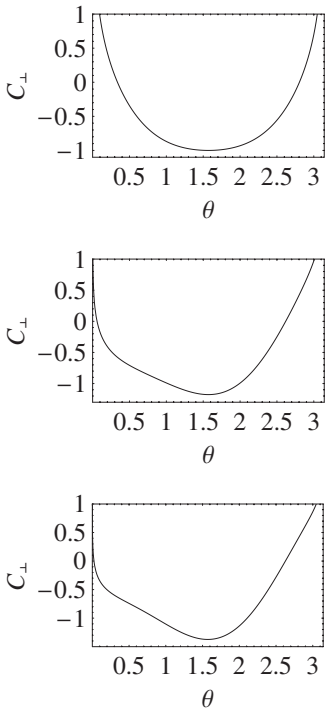

FIG. 4. $C_\perp$ vs Θ for three different values of ξ_0: $R_0=3$, $\xi_0=0$ (top); $R_0=3\sqrt{\mathcal{A}(0)/\mathcal{A}(2)}$, $\xi_0=2$ (middle); $R_0=3\sqrt{\mathcal{A}(0)/\mathcal{A}(3)}$, $\xi_0=3$ (bottom).

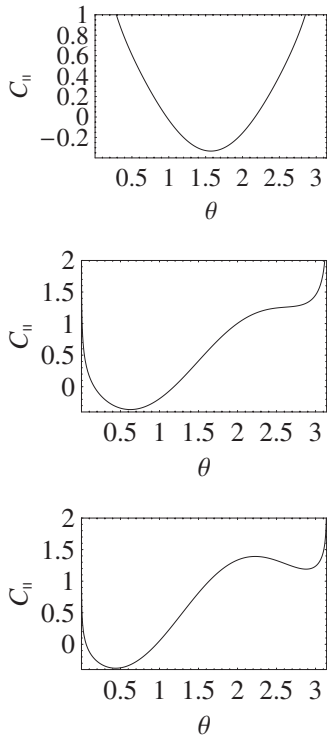

FIG. 5. $C_\parallel$ vs Θ: $R_0=3$, $\xi_0=0$ (top); $R_0=3\sqrt{\mathcal{A}(0)/\mathcal{A}(2)}$, $\xi_0=2$ (middle); $R_0=3\sqrt{\mathcal{A}(0)/\mathcal{A}(3)}$, $\xi_0=3$ (bottom).

$$C_\parallel,\ C_\perp \approx -\frac{2}{R_0}\log\left(\frac{R}{2R_0}\right). \tag{28}$$

The poles are umbilical points of the geometry, albeit in a singular way.

We will now show that this qualitative behavior holds for all values of ξ_0. However, a different strategy becomes more appropriate when $\xi_0 \neq 0$. We have the following exact expressions for the principal curvatures with respect to the parametrization given by Eq. (19)

$$\begin{aligned} C_\perp &= \frac{\partial_\Theta^2 R \partial_\Theta Z - \partial_\Theta^2 Z \partial_\Theta R}{[(\partial_\Theta R)^2 + (\partial_\Theta Z)^2]^{3/2}} \\ &= -\frac{1}{R_0}\left[3 + 2\cos\Theta\left(\log\tan\frac{\Theta}{2} + \xi_0\right)\right. \\ &\quad \left. + \sin^2\Theta\left(\log\tan\frac{\Theta}{2} + \xi_0\right)^2\right] \end{aligned} \tag{29}$$

and

$$\begin{aligned} C_\parallel &= -\frac{\partial_\Theta Z}{R[(\partial_\Theta R)^2 + (\partial_\Theta Z)^2]^{1/2}} \\ &= -\frac{1}{R_0}\left[1 + 2\cos\Theta\left(\log\tan\frac{\Theta}{2} + \xi_0\right)\right. \\ &\quad \left. - \sin^2\Theta\left(\log\tan\frac{\Theta}{2} + \xi_0\right)^2\right]. \end{aligned} \tag{30}$$

It is clear, by inspection, that the two principal curvatures diverge logarithmically at the poles $\Theta=0$ and $\Theta=\pi$. Note, however, that their difference remains finite with the value $C_\perp - C_\parallel = -2/R_0$ as consistency with Eq. (2) of [12] demands. The angular dependence of the curvatures for different values of ξ_0 is plotted in Figs. 4 and 5.

Note, in particular, how sharp the divergence is in the neighborhood of the south pole. Note also that both curvatures diverge to plus infinity. This peculiarity is associated with the logarithm; it is not visually apparent in the corresponding profiles due to the existence of a tangent plane (Fig. 2).

The singularity at the poles indicates that these surfaces, unlike the catenoid, require external forces along the axis of symmetry to support them.

It should be pointed out that the characteristic logarithmic singularity we have examined is, in fact, predicted by the linear theory. Consider the linear approximation to the Monge representation of the surface in terms of its height h above a plane. If the gradients of h are small, the bending energy H can be approximated by its quadratic part as

$$H \approx \frac{1}{2}\int d^2x (\nabla_\perp^2 h)^2, \tag{31}$$

where $\nabla_\perp$ is the gradient on the plane. The corresponding Euler-Lagrange equation is the biharmonic equation on the plane, $-(\nabla_\perp^2)^2 h = 0$. It is straightforward to show that the most general axially symmetric solution of this equation is given by

$$h = c_0 + c_1 R^2 \log R^2 + c_2 \log R + c_3 R^2. \tag{32}$$

The linear Monge approximation to the inverted catenoids is given by solutions with $c_0, c_2 = 0$. Of course, it is beyond the scope of this approximation to model their global behavior.

C. Singularities as manifestations of sources of stress

Axial symmetry dictates that the force on the membrane must be directed parallel to the axis, $\mathbf{F} = -2\pi c\mathbf{k}$. We have recently shown that c is the constant appearing in Eq. (2) of [12]. Thus using this equation and Eq. (7) we find that an inversion of the catenoid must satisfy the following equation:

$$C_\perp - C_\parallel = \frac{c|X|^2}{2R^2}. \tag{33}$$

If we now use the explicit expressions for the principal curvatures we identify $c = -4/R_0$. This is a reparametrization invariant measure of the singularity. It is also possible to see this directly using the expression given in Eq. (15): Without loss of generality, choose the contour to be a closed circle of polar radius R encircling the north pole. Now $\mathbf{l}$ is the tangent to the meridian and $ds = Rd\phi$. We do not use Eq. (13) which is ill-defined at the pole. Using Eqs. (10) and (28), and that on the north pole $\mathbf{n} = -\mathbf{k}$, we obtain

$$l_a \mathbf{f}^a = \frac{1}{2}(C_\perp^2 - C_\parallel^2)\mathbf{l} - (C_\perp + C_\parallel)'\mathbf{n} \approx (C_\perp + C_\parallel)'\mathbf{k} = \frac{4R_0}{R}\mathbf{k}. \tag{34}$$

As a consequence,

$$\mathbf{F} = 8\pi R_0 \mathbf{k}, \tag{35}$$

so that $c = -4/R_0$. The sign indicates that the force is always directed towards the interior.

D. Phases of a tethered membrane

We now possess a physical interpretation of the inverted geometry as an equilibrium with a pair of equal and opposite localized external forces applied at the poles holding them together. This might be compression applied outside, or the tension supplied by an internal tether. The curvature singularity at the poles is a manifestation of local forces. It is unrelated to the fact that they touch: They touch simply because all distant parts of the original catenoid get mapped to the origin, a peculiarity of the exact solution we have been handed.

The axial force and the reduced volume may be used to characterize axially symmetric compact shapes. The geometries with tethered poles that we have considered define a finite trajectory on this space illustrated in Fig. 6. Each point on this trajectory represents a specific geometry: the discocyte lies at one end (with the maximum force $c_1 = -4/3$), the limiting geometry consisting of a sphere within a sphere at the other (vanishing force $c_0 = 0$). The maximally inflated equilibrium geometry ($c_* = -0.712$) provides a natural division of the trajectory into two phases: discocytes and stomatocytes. The axial force may be interpreted as the order parameter describing the transition between these phases.

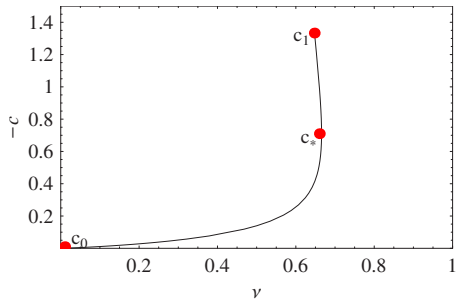

FIG. 6. (Color online) External force c vs v.

IV. DISCUSSION

The invariance of the bending energy of two-dimensional surfaces with respect to inversion is a curious symmetry whose physical consequences have only been touched on in this paper. We have focused on the inversion of a catenoid in a point along its axis, showing that it provides an exact description of a sequence of deflated topologically spherical equilibrium geometries with their poles tethered together by external forces. These forces are imprinted as curvature singularities on the membrane geometry.

In biology, the shape of membranes is very often controlled by external forces. Determining these shapes is a difficult problem and there are precious few analytical results. It is thus remarkable that conformal symmetry provides an exact analytical description of shape changing processes controlled by localized external forces.

We do not, of course, possess a lot of control over the shapes that inversion hands us: The poles touch. Intuitively, one would also expect that equilibrium shapes exist with poles held a finite distance apart. In the early nineties Ou-Yang Yhong-can, Naito, and Okuda identified an exact analogue of such configurations for a model with a finite spontaneous curvature [18]. While their paper does not discuss the external force needed to impose the constraint, this connection is clearly implied by the subsequent work of Podgornik, Svetina, and Žekš [13]. Analogous geometries do, in fact, also occur as equilibria of the conformally invariant system. A detailed description of these solutions is, however, beyond the scope of this paper. Inversion plays a role but in a somewhat more subtle way. Details will be presented in a forthcoming paper using the framework described in [12].

In general, the effect of external axial forces will be to pull out two cylindrical tubes or tethers. The physics of such tethers has been described using a more physically realistic Hamiltonian (see, for example, [19,20] and more recently [21,22]). While the physical system we have studied is the same, the membrane shapes we have described behave very differently. This is because the inversion symmetry we exploit forces us to look at a very different limit of the theory. The value for the reduced volume used in [19,20] is 0.95. In the limit we discuss, this value is outside the range assumed by a membrane with joined poles. More importantly, the sign of the forces differ. The forces holding the poles of our geometry together necessarily pull inward. This has an interesting consequence: the equilibrium area difference in our se-

quence turns out to be negative, a possibility which does not appear to have been contemplated previously. Perhaps this is because negative area differences do not arise in nonsingular axially symmetric geometries.

Of course, it would be interesting to explore the interpolation between these two sectors of the phase diagram. We hope to report on the details at a later date. The first step will be to study tube pulling in the conformally invariant system.

It is perhaps worth pointing out an important difference between the discocyte-stomatocyte transition we have described induced by external forces and that of a deflated fluid membrane induced by a change in the bilayer asymmetry. The latter has a long history dating back to Deuling and Helfrich's pioneering work in the 1970s [23] followed, after a long pause, by a burst activity beginning in the late 1980s (see, for example [24] as well as [3,25,26] for reviews). The bilayer asymmetry is captured by an energy penalty or constraint on the area difference between the two sheets. As a result, the conformal symmetry of the bending energy is broken at every point. In the inverted catenoid, on the other hand, there is no bilayer asymmetry. The localized external forces which induce the transition break conformal symmetry only at isolated points. As a consequence, it is possible to constrain the isoperimetric ratio without sacrificing the conformal invariance of the energy.

It is also perhaps worth stressing that two qualitatively identical geometries may correspond to very different physical conditions. The discocytes described in [18] are qualitatively indistinguishable from those described in [23]; this is because, visually, it is difficult to distinguish the behavior $h \sim -R^2 \log R$ from $h \sim R^2$ in the neighborhood of $R=0$; they differ in second derivatives. However, the divergent second derivative in the former signals the existence of a distributional external force. External forces leave their imprint on the local membrane geometry which will be picked up by the line integral of the stress tensor. In principle, it is always possible to reconstruct the distribution of external forces $\{\mathbf{F}_1, \ldots, \mathbf{F}_N\}$ acting on the membrane from a knowledge of the appropriate geometrical data (i.e., tangent vectors, normal, curvature, etc.) in the neighborhood of a sufficient number of surface contours.

We have yet to say anything about the stability of the shapes we have discussed. Expanding the bending energy out to second order in deformations about a minimal surface, one can show that [27]

$$H = \frac{1}{2} \int dA\, \Phi(-\nabla^2 + \mathcal{R})^2 \Phi, \tag{36}$$

where $\Phi = \delta\mathbf{X} \cdot \mathbf{n}$ is the normal deformation and $\mathcal{R}$ is the scalar curvature (twice the Gaussian curvature $C_1 C_2$). Remarkably, this expression depends only on intrinsic geometry. It also should be compared with the corresponding expression for the area,

$$H = \int dA\, \Phi(-\nabla^2 + \mathcal{R})\Phi. \tag{37}$$

In general, for any minimal surface $\mathcal{R} < 0$. Thus the catenoid spanning two rings becomes unstable as a minimal surface beyond a certain maximum separation. By contrast, note that the expression given by Eq. (36) is manifestly positive. Thus, if tension may be ignored, the same catenoid is stable as a Willmore surface. The conformal invariance of the energy should hold order by order in perturbations theory. This suggests that the inverted shapes are also stable. While one does need to check that there is no hidden subtlety associated with singularities, conformal invariance clearly simplifies the analysis of stability.

So much for axially symmetric configurations. It is clearly possible to generate nonaxially symmetric geometries held by a pair of tethers by inverting these geometries in any point off the axis of symmetry. It appears reasonable to conjecture that all equilibrium shapes with a pair of tethers are generated by inversion.

It is also clear, however, that there is much more to this story. For the catenoid is but the simplest of a vast and growing number of interesting minimal surfaces. How do we describe equilibria held in place by three or more tethers? It is not unreasonable to guess that the inversion of nonaxially symmetric minimal surfaces will play a role. We are currently examining the properties under inversion of the natural generalization of the catenoid, the k-noids of Jorge and Meeks [28]. This could provide a nonperturbative handle on yet another problem of interest in membrane biophysics: How does one identify the stable configurations assumed by proteins when the interaction between them is mediated by membrane curvature [29]?

ACKNOWLEDGMENTS

We have benefitted from conversations with Markus Deserno, Martin Müller, Francisco Solis, and Pablo Vazquez. We are also grateful for the hospitality of IPAM. Partial support from CONACyT Grant No. 51111 as well as DGAPA PAPIIT Grant No. IN119206-3 is acknowledged.

Appendix A

The tangent vectors adapted to the parametrization are $\mathbf{e}_a = \partial_a \mathbf{X}$ and $\mathbf{n}$ is the unit normal. The induced metric on the surface and the extrinsic curvature are given by $g_{ab} = \mathbf{e}_a \cdot \mathbf{e}_b$ and $K_{ab} = \mathbf{e}_a \cdot \partial_b \mathbf{n}$, respectively [30–32]. Indices are raised with the inverse metric g^{ab}. The element of area is given by $dA = \sqrt{\det g_{ab}}\, d^2u$. K denotes (twice) the mean curvature: $K = g^{ab} K_{ab}$.

Appendix B

The principal curvatures are given by

$$C_\perp = \bar{\Theta}', \quad C_\parallel = \sin\bar{\Theta}/\bar{R},$$

where $\bar{\Theta}$ denotes the angle that the tangent along the meridian makes with the planes of constant Z, and the prime denotes a derivative with respect to arc length along the meridian. The arc length is given by

$$ds^2 = (1 + Z_{,R}^2) dR^2.$$

Thus $\cos\bar{\Theta} = R' = -1/(1+Z_{,R}^2)^{1/2} \approx -1$, $\sin\bar{\Theta} = -Z' = Z_{,R}/(1+Z_{,R}^2)^{1/2} \approx Z_{,R}$, and $\bar{\Theta} \approx Z_{,RR}$.

[1] P. Canham, J. Theor. Biol. **26**, 61 (1970); W. Helfrich, Z. Naturforsch. C **28**, 693 (1973).
[2] R. Lipowsky and E. Sackmann, *Structure and Dynamics of Membranes*, Handbook of Biological Physics (Elsevier Science B. V., Amsterdam. 1995), Vols. 1 and 2.
[3] U. Seifert, Adv. Phys. **46**, 13 (1997).
[4] O. Mouritsen, *As a Matter of Fat* (Springer, New York, 2005).
[5] T. J. Willmore, *Total Curvature in Riemannian Geometry* (Ellis Horwood, Chichester, 1982).
[6] A. M. Polyakov, *Gauge Fields and Strings* (Harwood Academic Publishers, New York, 1987).
[7] U. Seifert, J. Phys. A **24**, L573 (1991); F. Jülicher, U. Seifert, and R. Lipowsky, Phys. Rev. Lett. **71**, 452 (1993).
[8] M. M. Müller, M. Deserno, and J. Guven, Europhys. Lett. **69**, 482 (2005); Phys. Rev. E **72**, 061407 (2005).
[9] R. Capovilla and J. Guven, J. Phys. A **35**, 6233 (2002).
[10] J. Guven, J. Phys. A **37**, L313 (2004).
[11] This should not be confused with a catenoid formed by a soap film spanning two rings which is under tension.
[12] P. Castro-Villarreal and J. Guven, J. Phys. A **40**, 4273 (2007).
[13] R. Podgornik, S. Svetina, and B. Žekš, Phys. Rev. E **51**, 544 (1995).
[14] J. H. White, Proc. Am. Math. Soc. **38**, 162 (1973).
[15] A. Gray, *Modern Differential Geometry of Curves and Surfaces with Mathematica* (Chapman & Hall/CRC, Boca Raton, FL, 2006).
[16] J. Guven, J. Phys. A **38**, 7943 (2005).
[17] J. Guven, J. Phys. A **39**, 3771 (2006).
[18] H. Naito, M. Okuda, and Ou-Yang Zhong-can, Phys. Rev. E **48**, 2304 (1993).
[19] B. Božič, S. Svetina, and B. Žekš, Phys. Rev. E **55**, 5834 (1997).
[20] V. Heinrich, B. Božič, S. Svetina, and B. Žekš, Biophys. J. **76**, 2056 (1999).
[21] I. Derenyi, F. Julicher, and J. Prost, Phys. Rev. Lett. **88**, 238101 (2002).
[22] T. R. Powers, G. Huber, and R. E. Goldstein, Phys. Rev. E **65**, 041901 (2002).
[23] H. J. Deuling and W. Helfrich, J. Phys. (France) **37**, 1335 (1976).
[24] S. Svetina, and B. Žekš, Eur. Biophys. J. **17**, 101 (1989); U. Seifert, K. Berndl, and R. Lipowsky, Phys. Rev. A **44**, 1182 (1991); L. Miao, B. Fourcade, M. Rao, M. Wortis, and R. K. P. Zia, *ibid.* **43**, 6843 (1991); L. Miao, U. Seifert, M. Wortis, and H. G. Döbereiner, Phys. Rev. E **49**, 5389 (1994).
[25] R. Lipowsky, Nature (London) **349**, 475 (1991).
[26] S. Svetina and B. Žekš, in *Nonmedical Applications of Liposomes*, edited by D. D. Lasic and Y. Barenholz (CRC, Boca Raton, FL, 1996).
[27] R. Capovilla, J. Guven, and J. A. Santiago, J. Phys. A **36**, 6281 (2003).
[28] M. Weber, *Classical Minimal Surfaces in Euclidean Space by Examples* (Clay Institute Summer School on Minimal Surfaces MSRI, 2003).
[29] K. S. Kim, J. Neu, and G. Oster, Biophys. J. **75**, 2274 (1998).
[30] M. Do Carmo, *Differential Geometry of Curves and Surfaces* (Prentice Hall, Englewood Cliffs, NJ, 1976).
[31] S. Montiel and A. Ros, *Curves and Surfaces* (American Mathematical Society, Providence, RI, 2005).
[32] M. Spivak, *A Comprehensive Introduction to Differential Geometry*, 2nd ed. (Publish or Perish, Berkeley, 1979), Vols. 1-5.